Hydrodynamic Theory of Partially Degenerate Electron-Hole Fluids in Semiconductors

M. Akbari-Moghanjoughi[1] and B. Eliasson[2]

[1]*Faculty of Sciences, Department of Physics,*

Azarbaijan Shahid Madani University, 51745-406 Tabriz, Iran

[2]*SUPA, Physics Department, John Anderson Building,*

University of Strathclyde, Glasgow G4 0NG, Scotland, UK

(Dated: 10 July 2016)

Abstract

A quantum hydrodynamic (QHD) theory for high-frequency electron-hole Langmuir and acoustic-like oscillations as well as static charge shielding effects in arbitrarily doped semiconductors is presented. The model includes kinetic corrections to the quantum statistical pressure and to the quantum Bohm potential for partially degenerate electrons and holes at finite temperatures. The holes contribute to the oscillations and screening effects in semiconductors in a similar manner as real particles. The dielectric functions are derived in the high-frequency limit for wave excitations and in the low-frequency limit for the study of static screening. The dispersion relation for the Langmuir and acoustic-like oscillations is examined for different parameters of doped silicon (Si). Some interesting properties and differences of electron hole dynamical behavior in N- and P-type Si are pointed out. Holes are also observed to enhance an attractive charge shielding effect when the semiconductor is highly acceptor-doped.

PACS numbers: 52.30.-q,71.10.Ca, 05.30.-d

I.   INTRODUCTION

The electron-hole dynamics governs the essential features of modern semiconductor devices and integrated circuits [1, 2]. Electron-hole plasmas play a fundamental role in the operation of high-speed and high-power semiconductor switches and oscillators such as high-gain resonant tunneling diodes (RTD), photoconductive semiconductor switches (PCSS), Read diodes, impact ionization avalanche transit time devices, Gunn oscillators and radiation detectors (RD) [4]. Modern technologies such as optoelectronics, spintronics, nanoelectronics, plasmonics, etc. [5, 6] can be modeled by hydrodynamic equations for charged carriers to study collective quantum transport phenomena in miniaturized devices. While the free electron and nearly free electron theories [7, 8] may be useful in describing physical properties of degenerate electron fluids in metals and semiconductors, the kinetic and hydrodynamic models are more appropriate for investigations of the collective dynamics including the electrostatic and electromagnetic interactions in quantum plasmas. Electronic polarizability, transport, transit time effects and resonances are collective phenomena that require frameworks beyond the single particle picture. Bohm, Pines and Levine [11–14] and Klimontovich and Silin [18] pioneered the theory of electron oscillations for degenerate electron systems. On the other hand, because of less complexity compared to density matrix, Wigner function, and density functional theories [15–17], quantum hydrodynamic models [9, 10] have been shown to be useful in describing the most essential quantum features of the system at the lowest complexity. Quantum hydrodynamic models derived from the Wigner-Poisson kinetic formulation and the Madelung quantum many-body representation [19, 20] have been extensively used to investigate the linear and nonlinear features of quantum plasmas [21, 22]. One of the interesting findings of the quantum hydrodynamic theory was the prediction of attractive forces between similar charges by degenerate electrons in quantum plasmas [23]. However, this feature of quantum plasmas has been the subject of an intense recent debate [24–31]. The study of quantum plasmas using the hydrodynamic model [32] is relevant to the partially or completely degenerate electron fluids in which the electron de Broglie thermal wavelength is of the same order or larger than the mean inter-electron distance leading to a Fermi-Dirac instead of a Maxwell-Boltzmann distribution of electrons, or when the size of the system under study (e.g. the wavelength of a wave) is comparable with the de Broglie wavelength. The zero-temperature limit used in earlier quantum hydrodynamic

theory has been extended to include finite temperatures in the recent kinetically modified quantum hydrodynamic theory for arbitrary electron degeneracy [33–35]. The application of the generalized model for static charge screening has been shown to be consistent with the gradient-corrected Thomas-Fermi model [36, 39].

The aim of this paper is to use a finite temperature quantum fluid model to study electrostatic waves and static screening in semiconductor electron-hole plasmas. The paper is organized in the following fashion. In Sec. II, we develop the hydrodynamic model of an arbitrarily degenerate electron-hole quantum plasma including the most important kinetic corrections. The linearized dielectric function for waves in a finite temperature plasmas is obtained in Sec III by including the kinetic correction prefactor of the quantum statistical pressure, and the high-frequency Langmuir excitations and acoustic-like waves in an electron-hole fluid in semiconductors are studied. The static charge shielding is investigated in Sec. IV. Finally, a summary is presented in Sec. V.

II.   GENERALIZED QUANTUM HYDRODYNAMICS MODEL

Let us consider an electron fluid in a collisionless neutralizing background of doped semiconducting ions. At equilibrium, the electrons and hole densities are in balance between generation rate ν_g and recombination rate ν_r. These rates will be neglected in the dynamical model below with the assumptions that the recombination/generation frequencies (typically $10^6 \mathrm{s}^{-1}$ for silicon at room temperature) are much smaller than the typical oscillation frequency (cf. Sect. III) and that the mean free path (typically 22nm for silicon at room temperature) is much longer than typical shielding lengths (cf. Sect. IV). The dynamics of the electron-hole fluid perturbations can then be modeled through the quantum hydrodynamic model incorporating the continuity and the generalized momentum equations for particle species s with $s = e$ for electrons and $s = h$ for holes, coupled with Poisson's equation for the potential, as

$$\frac{\partial n_s}{\partial t} + \nabla \cdot (n_s \mathbf{u}_s) = 0, \tag{1a}$$

$$\frac{\partial \mathbf{u}_s}{\partial t} + (\mathbf{u}_s \cdot \nabla)\mathbf{u}_s + \nu_{is}\mathbf{u}_s = \frac{q_s}{m_s^*}\nabla\phi - \frac{\nabla P_s}{n_s m_s^*} + \frac{\xi_s \hbar^2}{6 m_s^{*2}}\nabla\left(\frac{\Delta \sqrt{n_s}}{\sqrt{n_s}}\right), \tag{1b}$$

$$\Delta\phi = 4\pi e\left(n_e - n_h + N\right), \tag{1c}$$

where q_s is the magnitude of the charge with $q_e = -e$ and $q_h = +e$ and e being the magnitude of the electron charge, m_s^* is the effective particle mass, $\hbar$ is Planck's constant divided by 2π, n_s is the number density of each species, P_s is the statistical pressure, and $N = N_a - N_d$ with N_a and N_d being the number densities of the acceptor and donor ions, respectively. The last term in the left-hand side of the carrier momentum balance equation accounts for the carrier-phonon collision phenomenon (ν_{is} being the carrier-phonon collision frequency) which will be ignored in this analysis for simplicity. However, the generalized hydrodynamic model including the carrier-phonon collisions can be easily treated in the presence of a detailed knowledge on the temperature and doping concentration dependence of carrier mobilities [1]. It is also realistic to consider the ballistic transport in recent devices with sizes less than carrier mean-free paths. Other derivation of the quantum hydrodynamics model of semiconductors accounting for the carrier-phonon collisions can be found in Ref. [37]. Also a generalized hydrodynamics model for semiconductors based on the maximum entropy principle which includes the quantum corrections appears in [38]. Also, the last term on the right-hand side of Eq. (1b) is due to quantum tunneling of the electrons and holes (sometimes called the Bohm potential), where ξ_s is a kinetic correction [33]. The equation of state (EoS) of the electrons and holes to be used in the hydrodynamic model needs particular attention due to the fact that the compression of the quantum gas can either be low or high frequency, and we will denote the pressure $P_s = P_s^{(is)}$ and $P_s = P_s^{(ad)}$ for isothermal and adiabatic fluid compression, respectively.

Figure 1 shows the energy band diagram for a typical semiconductor, where E_F is the equilibrium Fermi energy of the system and E_c and E_v are respectively the conduction and valence energies of the semiconductor, μ_e and μ_h are the electron and hole chemical potentials, and E_g is the gap energy. The Fermi energy indicates the energy required to add an electron ($\mu_e = E_F - E_c < 0$) or hole ($\mu_h = E_F - E_v > 0$) to the system, where $\mu_{h0} - \mu_{e0} = E_c - E_v = E_g > 0$ with μ_{h0} and μ_{e0} being the equilibrium values of hole and electron chemical potentials. The number density of species s is obtained by integrating the product of the density of states (DoS) and the Fermi-Dirac probability function over energy
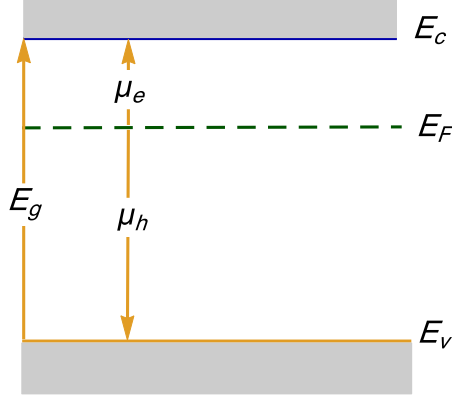
FIG. 1: The energy-band diagram of a semiconductor showing the valence and conduction bands E_v and E_c, the Fermi energy E_F, the chemical potentials μ_e and μ_h of the electrons and holes, respectively, and the gap-energy E_g of the semiconductor.

as [1–3]

$$n_e = \frac{2^{1/2}m_e^{*3/2}}{\pi^2\hbar^3}\int_{E_c}^{+\infty}\frac{\sqrt{E-E_c}\,dE}{e^{\beta(E-E_F)}+1} = \frac{2^{1/2}m_e^{*3/2}}{\pi^2\hbar^3}\int_0^{+\infty}\frac{\sqrt{\mathcal{E}}\,d\mathcal{E}}{e^{\beta(\mathcal{E}+E_c-E_F)}+1}, \qquad (2a)$$

$$n_h = \frac{2^{1/2}m_h^{*3/2}}{\pi^2\hbar^3}\int_{-\infty}^{E_v}\frac{\sqrt{E_v-E}\,dE}{e^{\beta(E_F-E)}+1} = \frac{2^{1/2}m_h^{*3/2}}{\pi^2\hbar^3}\int_{-\infty}^0\frac{\sqrt{-\mathcal{E}}\,d\mathcal{E}}{e^{\beta(E_F-E_v-\mathcal{E})}+1}, \qquad (2b)$$

where $\beta = 1/(k_BT)$, and we used a change of integration variable $E - E_c = \mathcal{E}$ in Eq. (2a) and $E - E_v = \mathcal{E}$ in Eq. (2b). Using the definitions of the chemical potentials $\mu_e = E_F - E_c$ and $\mu_h = E_F - E_v$ gives

$$n_e = \frac{2^{1/2}m_e^{*3/2}}{\pi^2\hbar^3}\int_0^{+\infty}\frac{\sqrt{\mathcal{E}_e}\,d\mathcal{E}_e}{e^{\beta(\mathcal{E}_e-\mu_e)}+1}, \qquad (3a)$$

$$n_h = \frac{2^{1/2}m_h^{*3/2}}{\pi^2\hbar^3}\int_0^{+\infty}\frac{\sqrt{\mathcal{E}_h}\,d\mathcal{E}_h}{e^{\beta(\mathcal{E}_h+\mu_h)}+1}, \qquad (3b)$$

where we also made a change of sign of the integration variable, $\mathcal{E} = -\mathcal{E}_h$, in Eq. (3b).

For waves with very low phase speeds compared to the mean particle speed, or for static screening of a test charge, the electrons and holes have the time to stream and reach equilibrium to screen the perturbations. In this case, the compression can be considered to be isothermal (β =constant), and the equation of state (EoS) reads (e.g. [33])

$$P_s^{(is)} = \frac{2^{3/2}m_e^{*3/2}}{3\pi^2\hbar^3}\int_0^{+\infty}\frac{\mathcal{E}_e^{3/2}\,d\mathcal{E}_e}{e^{\beta(\mathcal{E}_e-\mu_e)}+1}, \qquad (4a)$$

$$P_s^{(is)} = \frac{2^{3/2}m_h^{*3/2}}{3\pi^2\hbar^3}\int_0^{+\infty}\frac{\mathcal{E}_h^{3/2}\,d\mathcal{E}_h}{e^{\beta(\mathcal{E}_h+\mu_h)}+1}. \qquad (4b)$$

5

Carrying out the integrals, Eqs. (3a,b) and (4a,b) can be expressed as

$$n_s = -N_s \mathrm{Li}_{3/2}\left[-\exp\left(\pm\beta\mu_s\right)\right], \quad P_s^{(is)} = -\frac{N_s}{\beta}\mathrm{Li}_{5/2}\left[-\exp\left(\pm\beta\mu_s\right)\right], \tag{5}$$

where $\mathrm{Li}_\nu(z)$ is the polylogarithm function of the order ν and the argument z, and where the upper/lower sign is for the electrons/holes. Here, the effective densities of states for the electrons and holes are given by [1]

$$N_e = \frac{2}{\Lambda_e^3} = 2\left(\frac{m_e^*}{2\pi\beta\hbar^2}\right)^{3/2}, \quad N_h = \frac{2}{\Lambda_h^3} = 2\left(\frac{m_h^*}{2\pi\beta\hbar^2}\right)^{3/2}, \tag{6}$$

where Λ_s is the electron(hole) de Broglie thermal wavelength. The EoS (5) can then be written

$$P_s^{(is)} = \frac{n_s}{\beta}\frac{\mathrm{Li}_{5/2}[-\exp(\pm\beta\mu_s)]}{\mathrm{Li}_{3/2}[-\exp(\pm\beta\mu_s)]} \tag{7}$$

A similar EoS as Eq. (7) has been used for the electrons to study low-frequency ion-acoustic waves in an electron-ion quantum plasma [33].

In the opposite limit, for electrostatic waves with wave speeds much higher than the average particle speed, the electrons and holes do not have the time to stream and reach an equilibrium. The distribution in phase space (velocity, space) then behaves to first order as an incompressible phase-fluid [35] governed by a collisionless Boltzmann (Vlasov) equation, and where the chemical potential must be constant for one-dimensional compression. This leads to the adiabatic EoS

$$P_s^{(ad)} = \frac{n_{s0}G_s}{\beta}\left(\frac{n_s}{n_{s0}}\right)^3, \tag{8}$$

with the equilibrium number density, temperature and chemical potential related through

$$n_{s0} = -N_s \mathrm{Li}_{3/2}\left[-\exp\left(\pm\beta\mu_{s0}\right)\right], \tag{9}$$

and we denoted

$$G_s = \frac{\mathrm{Li}_{5/2}[-\exp(\pm\beta\mu_{s0})]}{\mathrm{Li}_{3/2}[-\exp(\pm\beta\mu_{s0})]}. \tag{10}$$

In the language of thermodynamics, the exponent 3 in Eq. (8) may be interpreted as the adiabatic index $\gamma = (D+2)/D$ with the number of degrees of freedom $D = 1$ for one-dimensional adiabatic compression [19, 35]. For this case, we also have $\xi_s = 3$.

At equilibrium, the number densities of the electrons and holes are related to the intrinsic number density n_i via the mass-action law $n_{e0}n_{h0} = n_i^2$. In the presence of arbitrary

doping the equilibrium values of the number densities are given through the generalized semiconductor theory [1] as

$$n_{e0} = -\frac{N}{2} + \left(\frac{N^2}{4} + n_i^2\right)^{1/2}, \quad n_{h0} = \frac{N}{2} + \left(\frac{N^2}{4} + n_i^2\right)^{1/2}.$$
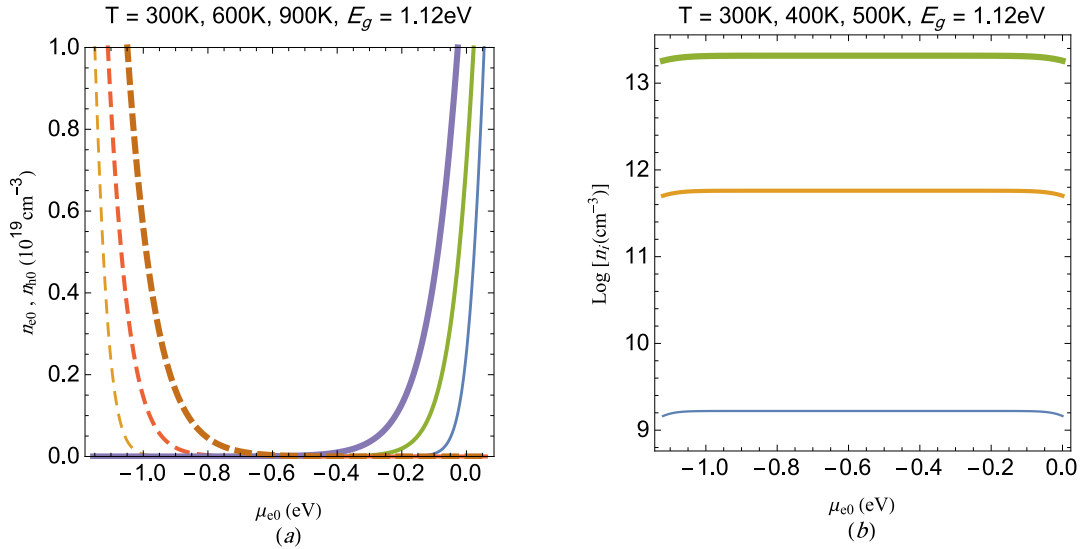
(11)

The mass-action law then reads

FIG. 2: (a) The electron (solid) and hole (dashed) equilibrium number densities as functions of the equilibrium electron chemical potential μ_{e0} for different temperatures T. (b) Dependence of the intrinsic number density n_i with T. Thicker curves indicate higher values of T listed above each panel.

$$n_i = \sqrt{N_e N_h \text{Li}_{3/2}\left[-\exp\left(\beta\mu_e\right)\right]\text{Li}_{3/2}\left[-\exp\left(-\beta\mu_h\right)\right]},$$

(12)

where in the classical limit $\beta\mu_e \ll -1$ and $\beta\mu_h \gg +1$, we have $\text{Li}_{3/2}[-\exp(\beta\mu_e)] \approx -\exp(\beta\mu_e)$ and $\text{Li}_{3/2}[-\exp(-\beta\mu_h)] \approx -\exp(-\beta\mu_h)$, and Eq. (12) reduces to $n_i = \sqrt{N_e N_h}\exp[\beta(\mu_e - \mu_h)/2] = \sqrt{N_e N_h}\exp(-\beta E_g/2)$ [1]. Note that $\mu_{e0} < 0$ and $\mu_{h0} > 0$ for nondegenerate semiconductors. For the case of an N-type $(N_d - N_a \gg n_i)$ semiconductor such as Arsenic-Boron doped silicon (Si) with $N_A > N_B$, we have $n_{e0} \simeq N_d - N_a$ and $n_{h0} = n_i^2/n_{e0}$, and for P-type $(N_a - N_d \gg n_i)$ semiconductor with $N_B > N_A$, we have $n_{h0} \simeq N_a - N_d$ and $n_{e0} = n_i^2/n_{h0}$. We note that for a nondegenerate intrinsic $(N = 0)$ semiconductors, the equilibrium chemical potential relation $\mu_{e0} = -\mu_{h0} = -E_g/2$ (with

$n_{e0} = n_{h0} = n_i$) holds for the electron-hole fluid, due to balance between electron-hole generation and recombination. Also, for a given temperature but varying doping concentration, the relation $\mu_{h0} - \mu_{e0} = E_g$ is satisfied in general for extrinsic ($N \neq 0$) semiconductors.

Figure 2(a) shows the variation of the equilibrium electron and hole number densities n_{e0} and n_{h0} as functions of the electron chemical potential μ_{e0} for different temperatures T in an undoped Si semiconductor with $m_e^* = 0.26m_0$, $m_h^* = 0.36m_0$ and $E_g = 1.12$eV (There are two different definitions for carrier effective mass [43], namely, effective mass for DoS calculations and that for conductivity calculations. The longitudinal and transverse electron effective masses of electrons in silicon are respectively $m_{el}^* = 0.89m_0$ and $m_{et}^* = 0.19m_0$ which lead to the conductivity effective mass of $m_{ec}^* = 3/(1/m_{el}^* + 2/m_{et}^*) = 0.26m_0$). The equilibrium electron chemical potential is negative for low number densities ($n_{e0} < 10^{20}$cm^{-3}) corresponding to non-degenerate electrons. An increase of the temperature leads to an increase of both n_{e0} and n_{h0}. However, the mass-action law dictates that n_{e0} is low when n_{h0} is high, and *vice versa*. Figure 2(b) shows the intrinsic number density n_i of Si as a function of μ_{e0} for different temperatures. It is seen that except for μ_{e0} very close zero or to the gap-energy, the value of n_i is nearly independent of μ_{e0}, while it increases significantly with increasing temperature.

III.   ELECTRON-HOLE LANGMUIR AND ACOUSTIC-LIKE OSCILLATIONS

In order to study high frequency electron-hole excitations in semiconductors one may use the model (1) with $\xi_s = 3$, together with the EoS (8) for adiabatic compression of the electron-hole fluid as

$$\frac{\partial n_s}{\partial t} + \nabla \cdot (n_s \mathbf{u}_s) = 0, \tag{13a}$$

$$\frac{\partial \mathbf{u}_s}{\partial t} + (\mathbf{u}_s \cdot \nabla)\mathbf{u}_s = \frac{q_s}{m_s^*}\nabla\phi - \frac{n_{s0}V_{Ts}^2 G_s}{n_s}\nabla\left(\frac{n_s}{n_{s0}}\right)^3 + \frac{\hbar^2}{2m_s^{*2}}\nabla\left(\frac{\Delta\sqrt{n_s}}{\sqrt{n_s}}\right), \tag{13b}$$

$$\Delta\phi = 4\pi e \left(n_e - n_h + N\right), \tag{13c}$$

where $V_{Ts} = \sqrt{k_B T/m_s^*}$ is the thermal speed. Next, we linearize the system by using $n_s = n_{s0} + n_{s1}$, $u = u_1$ and $\phi = \phi_1$ and Fourier analyze the system by assuming a plane-wave perturbation for the first order linear quantities, so that n_{s1}, u_{s1}, and ϕ_1 are proportional to $\exp(i\mathbf{k} \cdot \mathbf{r} - i\omega t)$. The dielectric function of the electron-hole system is of the form

$D(k, \omega) = 1 + \chi_e + \chi_h$ with the electron and hole susceptibilities χ_s given by

$$\chi_s = \frac{\omega_{ps}^2}{\hbar^2 k^4 / (4m_s^{*2}) + 3V_{Ts}^2 G_s k^2 - \omega^2}. \tag{14}$$

For a pure electron gas without holes ($\omega_{ph} = 0$), the dispersion relation $1 + \chi_e = 0$ recovers wave frequencies of the Langmuir oscillations in the non-degenerate classical ($\beta\mu_{e0} \ll -1$) and fully degenerate quantum ($\beta\mu_{e0} \gg 1$) limits [35] as

$$\omega_c = \left(\omega_{pe}^2 + 3V_{Te}^2 k^2 + \frac{\hbar^2 k^4}{4m_e^{*2}} \right)^{1/2}, \quad \omega_q = \left(\omega_{pe}^2 + \frac{3}{5}V_{Fe}^2 k^2 + \frac{\hbar^2 k^4}{4m_e^{*2}} \right)^{1/2}, \tag{15}$$

where $V_{Fe} = \sqrt{2E_{Fe}/m_e^*}$ is the Fermi speed and $E_{Fe} = (\hbar^2/2m_e^*)(3\pi^2 n_{e0})^{2/3}$ is the electron Fermi energy. In the high-temperature classical limit, the quantum term $\hbar^2 k^4 / 4m_e^2$ can usually be neglected, and the classical Bohm-Gross dispersion relation of the Langmuir excitations is retained.

It is observed that the high frequency dielectric function of semiconductors is calculated using Eq. (14) in terms of electron and hole equilibrium chemical potentials, $\mu_{e0}(N, E_g, T)$ and $\mu_{h0}(N, E_g, T)$ for a given doping scheme, gap-energy and temperature. The generalized mass-action law, using Eqs. (5), (11) and (12), can be written

$$N_e \text{Li}_{3/2} \left[-\exp(\beta\mu_{e0}) \right] - N_h \text{Li}_{3/2} \left\{ -\exp\left[-\beta(E_g + \mu_{e0}) \right] \right\} = N. \tag{16}$$

Moreover, writing the dielectric function as

$$D(k, \omega) = 1 + \frac{1}{C_e - D_e\omega^2} + \frac{1}{C_h - D_h\omega^2}, \tag{17}$$

where $C_s = A_s k^4 + B_s k^2$, $A_s = \hbar^2/(4m_s^{*2}\omega_{ps}^2)$, $B_s = 3G_s V_{Ts}^2/\omega_{ps}^2$, and $D_s = 1/\omega_{ps}^2$, the solutions of the dispersion relation $D(k, \omega) = 0$ are given by

$$\omega = \frac{1}{\sqrt{2}} \sqrt{ \left(\frac{C_e + 1}{D_e} + \frac{C_h + 1}{D_h} \right) \pm \sqrt{ \left(\frac{C_e + 1}{D_e} - \frac{C_h + 1}{D_h} \right)^2 + \frac{4}{D_e D_h} } }, \tag{18}$$

where the positive and negative signs under the square root are associated with a Langmuir- and acoustic-like branch, respectively. The occurrence of such branches is a well-known characteristics of pair plasmas [40, 41] such as electron-ion, electron-positron and pair-ion plasmas. The Langmuir and acoustic branches have been discussed in the past for classical equal-mass plasmas [42], electron-positron plasmas [44], and for semiconductor electron-hole
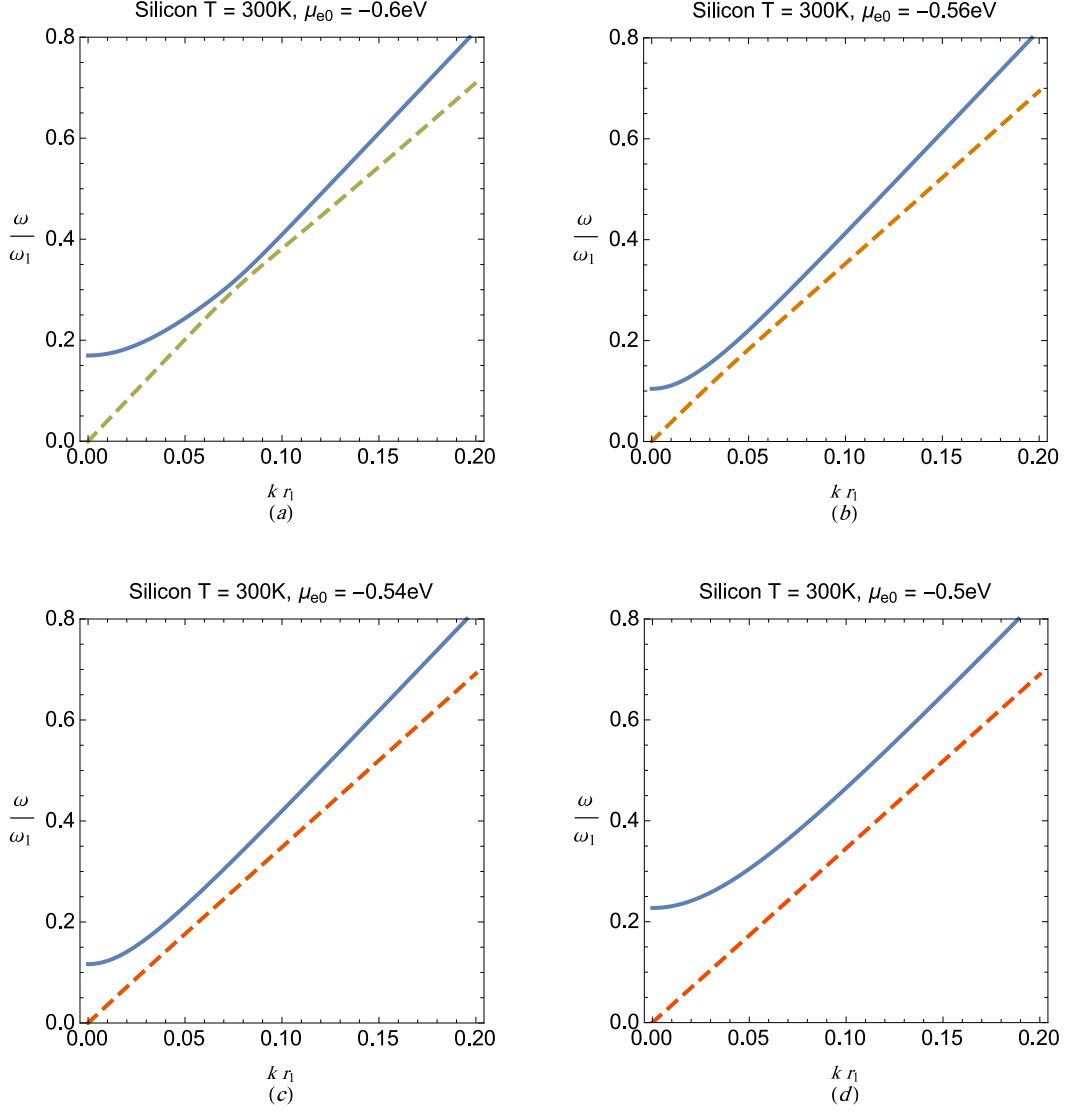
9

FIG. 3: Dispersion curves for electron-hole oscillations in doped Si ($E_g = 1.12$eV, $m_e = 0.26m_0$ and $m_h = 0.36m_0$ with m_0 being the free electron mass). Panels show the dispersion curve for various values of electron chemical potential. The normalization factors are $r_1 = 10^{-4}$cm and $\omega_1 = \sqrt{4\pi e^2 n_0/m_0}$ with $n_0 = 10^{12}$cm^{-3}. The solid and dashed profiles correspond to Langmuir and acoustic-like mode, respectively.

plasmas using a collective Schrödinger model [45]. In classical pair plasmas, however, the acoustic branch is heavily damped [44] due to phase-mixing of particles.

Figure 3 shows dispersion curves for a silicon electron-hole fluid for different values of μ_{e0} at $T = 300$ K. The existence of two branches is apparent of which one is acoustic-like (shown as dashed) and the other Langmuir-like (shown as solid). Figure 5(a) shows the dispersion

in P-type Si with $\mu_{e0} = -0.6$eV. As the electron chemical potential value is increased (the sample becomes N-type by introducing donor atoms like As) by going from plot (a) via (b) to (d) with $\mu_{e0} = -0.5$eV, it is seen that the two branches have almost equal frequencies at $k \approx 0.12 r_1^{-1}$. This proximity of the modes can become even more pronounced as the Fermi level approaches the valence band. Similar effects have been reported in other studies on pair-charged plasmas [40, 42].

Figure 4(a) shows the cutoff frequency at $k = 0$ for the electron-hole Langmuir branch in Si with respect to μ_{e0} for different values of T. The frequency has a minimum at the mid-gap for all temperatures. It is also observed that in both N-type ($\mu_{e0} > -0.56$eV) and P-type ($\mu_{e0} < -0.56$eV) Si the frequency increases exponentially with $|\mu_{e0} + 0.56$eV$|$. Figure 4(b) shows the plateau-like variation of the group speed (with respect to the electron equilibrium chemical potential) for the acoustic-like branch for $k = 0.1 r_1^{-1}$ at different values of T. Here, the group speed increases for all values of μ_{e0} (equivalently the doping concentration) with increasing temperature. It is also seen that the group speeds of the acoustic-like oscillations are higher in the P-type region compared to the N-type region (This feature is directly related to the effective masses of electrons and holes, where, for higher electron effective mass semiconductors the group speeds of the acoustic-like oscillations are higher in the N-type region compared to the P-type region). This shows the asymmetrical behavior of electron-hole oscillations in regions with different doping types. It is further observed that the group speed of the acoustic-like branch is nearly independent of μ_{e0} at each semiconductor doping region. In Fig. 4(c), we show the group speed of the Langmuir branch versus μ_{e0} for $k = 0.1 r_1^{-1}$ and different values of T. The group speed has a maximum at approximately the mid-gap point of the semiconductor. However, contrary to that of the acoustic like branch, the amplitude/width of the maximum decreases/increases sharply with increasing temperature. The asymmetry between the N- and P-type regions are also apparent in Fig. 4(c), and this asymmetry is even more pronounced for higher values of the wavenumber as seen in Fig. 4(d). Hence, Figs. 4(b)-(c) clearly illustrate the differences in the dynamics of electron-hole oscillations in N- and P-type semiconductors.

IV. THE STATIC CHARGE SHIELDING BY ELECTRONS AND HOLES

Let us now study the static limit of the dielectric function of an electron-hole liquid for arbitrary doping and finite temperature. In doing so, we use the low-frequency kinetic corrected quantum hydrodynamic model as given in Ref. [33] and the isothermal EoS (7). Using the identity $\nabla P_s^{(is)} = \pm n_s \nabla \mu_s$, the set of closed hydrodynamic equations for electron and hole species read

$$0 = \pm e \nabla \phi \mp \nabla \mu_s + \frac{\xi_s \hbar^2}{6m_s^*} \nabla \left(\frac{\nabla^2 \sqrt{n_s}}{\sqrt{n_s}} \right), \tag{19a}$$

$$\nabla^2 \phi = 4\pi e \left[n_e - n_h + N - Z\delta(\mathbf{r}) \right], \tag{19b}$$

where Z is the charge state of the test charge, $\delta(\mathbf{r})$ is Dirac's delta-function and the zeroth order low-frequency correction factor to the Bohm diffraction term is given by

$$\xi_{s0} = \frac{\mathrm{Li}_{3/2}\left[-\exp\left(\pm \beta \mu_{s0} \right) \right] \mathrm{Li}_{-1/2}\left[-\exp\left(\pm \beta \mu_{s0} \right) \right]}{\mathrm{Li}_{1/2}[-\exp\left(\pm \beta \mu_{s0} \right)]^2}. \tag{20}$$

Figure 5(a) shows the variation of ξ_{e0} versus μ_{e0} for different values of T. For a given value of T, the value of ξ_{e0} decreases from the limiting classical value of $\xi_{s0} = 1$ for $\beta\mu_{e0} \ll -1$ to the limiting fully degenerate value $\xi_{s0} = 1/3$ for $\beta\mu_{e0} \gg 1$. However, for $-E_g \leq \mu_{s0} \leq 0$ we have $0.795 \leq \xi_{e0} \leq 1$ for all temperatures and semiconductor gap-energies. The step-like vertical profile in Fig. 5(a) indicates the value of ξ_{e0} as a function of μ_{e0} at $T = 0$. Figure 5(b) shows the ξ_{e0} (solid curve) and ξ_{h0} (dashed curve) at $T = 300\,\mathrm{K}$. Linearizing and Fourier analyzing the system of Eqs. (19), we arrive at the static dielectric function

$$D_\xi(k,0) = 1 + \chi_e + \chi_h, \tag{21}$$

where the electron and hole susceptibilities are given by

$$\chi_s = \frac{\omega_{ps}^2}{\xi_{s0}\hbar^2 k^4/(12m_s^{*2}) + v_{Ts}^2 k^2}, \tag{22}$$

and we introduced the generalized thermal speed

$$v_{Ts} = V_{Ts}\sqrt{\frac{\mathrm{Li}_{3/2}\left[-\exp(\pm\beta\mu_{s0}) \right]}{\mathrm{Li}_{1/2}\left[-\exp(\pm\beta\mu_{s0}) \right]}}, \quad V_{Ts} = \sqrt{\frac{k_B T}{m_s^*}} \tag{23}$$

For the case of highly doped N-type ($N_d \gg N_a$) and P-type ($N_a \gg N_d$) semiconductors, it is observed that $\chi_e \gg \chi_h$ and $\chi_h \gg \chi_e$, respectively. Hence, the static dielectric function

simplifies significantly in these limiting cases, and we obtain, respectively,

$$D_{Nhd}(k,0) \simeq 1 + \frac{\omega_{pe}^2}{\xi_{e0}\hbar^2 k^4/(12m_e^{*2}) + v_{Te}^2 k^2}, \tag{24a}$$

$$D_{Phd}(k,0) \simeq 1 + \frac{\omega_{ph}^2}{\xi_{h0}\hbar^2 k^4/(12m_h^{*2}) + v_{Th}^2 k^2}. \tag{24b}$$

The corresponding screening potential is of the general form [23]

$$\phi(r) = \frac{Ze}{2\pi^2}\int\frac{\exp(ikr)}{k^2 D(k,0)}d^3k = \frac{Ze}{2r}\left[(1+b)\,e^{-k_+ r} + (1-b)\,e^{-k_- r}\right]. \tag{25}$$

The potential given in Eq. (25) with the dielectric function given by either Eq. (24a) or (24b) is known to admit repulsive and attractive forms [36]

$$\phi_r(r) = (Ze/r)\exp(-Ar)\left[\cosh(Br) + b\sinh(Br)\right], \quad \eta_s < \frac{1}{4}, \quad 1 < b < \infty, \tag{26a}$$

$$\phi_a(r) = (Ze/r)\exp(-A'r)\left[\cos(B'r) + b'\sin(B'r)\right], \quad \eta_s > \frac{1}{4}, \quad 0 < b' < \infty, \tag{26b}$$

where the parameters are defined as

$$A = k_{0s}\frac{\sqrt{\sqrt{4\eta_s}+1}}{\sqrt{4\eta_s}}, \quad B = k_{0s}\frac{\sqrt{1-\sqrt{4\eta_s}}}{\sqrt{4\eta_s}}, \quad b = \frac{1}{\sqrt{1-4\eta_s}}, \tag{27a}$$

$$A' = k_{0s}\frac{\sqrt{\sqrt{4\eta_s}+1}}{\sqrt{4\eta_s}}, \quad B' = k_{0s}\frac{\sqrt{\sqrt{4\eta_s}-1}}{\sqrt{4\eta_s}}, \quad b' = \frac{1}{\sqrt{4\eta_s-1}}, \tag{27b}$$

and $\eta_s = \xi_{s0}\hbar^2\omega_{ps}^2/(12m_s^{*2}v_{Ts}^2)$ and $k_{0s} = \omega_{ps}/v_{Ts}$.

In Fig. 6(a), we show the profiles of the screening potential in highly doped N-Type Si for various doping concentration. This potential is of non-oscillatory repulsive type given in Eq. (26a). The screening becomes more effective (screening length decreases) as the doping concentration increases. This trend also appears for highly doped P-Type Si in Fig 6(b) which is also of repulsive type. It is observed that the screening effect by holes in acceptor concentrated semiconductor samples is as effective as that of electrons in an N-type semiconductors. An even more striking effect concerning the screening by holes is seen in Fig. 6(c) which indicates that in a highly acceptor-doped semiconductor the oscillatory attractive screening is more pronounced than that of electrons in highly doped N-type semiconductors with similar doping scheme. This is an interesting property of electron-hole static charge screening in doped semiconductors with many possible implications in semiconductor science and technology. For example, the dynamics and mobility of carriers in semiconductors, and hence the device operation, is directly related to the electric permittivity. The static charge

13

shielding is of main concern in fabrication of integrated semiconductor devices and is important in the response of semiconductor detectors to external electrostatic or electromagnetic perturbations.

V. SUMMARY

We have presented a QHD theory for the investigation of high-frequency electron-hole oscillations in semiconductors and static charge shielding by electrons and holes by taking into account the kinetic corrections to the finite temperature chemical potential and quantum diffraction effects in the hydrodynamic model. It is found that holes contribute to the dynamics of oscillations and screening in semiconductors as effective as the electron fluid. Examination of the linear dispersion relation shows the appearance of both a Langmuir branch and an acoustic-like branch in the wave spectrum. The acoustic-like mode has some interesting features regarding the asymmetric behavior in N- and P-type semiconductors. An attractive screening potential also exists for some plasma parameters, and the attractive potential is more pronounced in highly acceptor-doped P-type semiconductors than in highly donor-doped N-type semiconductors with similar doping concentration.

VI. ACKNOWLEDGEMENTS

[1] C. Hu, *Modern Semiconductor Devices for Integrated Circuits* (Prentice Hall, Upper Saddle River, New Jersey, 2010) 1st ed.

[2] K. Seeger, *Semiconductor Physics* (Springer, Berlin, 2004) 9th ed.

[3] B. Van Zeghbroeck, *Principles of Electronic Devices* (2011), Chap. 2.5, http://ecee.colorado.edu/~bart/book/contents.htm

[4] F. J. Zutavern, A. G. Baca, W. W. Chow, M. J. Hafich, H. P. Hjalmarson, G. M. Loubriel, A. Mar, M. W. O'malley, and A. G. A. Vawter, in IEEE Conf. Pulsed Power Plasma Science (2001) doi:10.1109/PPPS.2001.961051.

[5] H. Haug and S. W. Koch, *Quantum Theory of the Optical and Electronic Properties of Semi-conductors* (World Scientific, Singapore, 2004).

[6] P. A. Markovich, C.A. Ringhofer, and C. Schmeister, *Semiconductor Equations* (Springer, Berlin, 1990).

[7] C. Kittel, *Introduction to Solid State Physics*, (John Wiely & Sons, New York, 1996), 7th ed.

[8] N. W. Ashcroft and N. D. Mermin, *Solid state physics* (Saunders College Publishing, Orlando, 1976).

[9] C. L. Gardner, SIAM J. Appl. Math. **54**, 409 (1994).

[10] C. L. Gardner, C. Ringhofer, Phys. Rev. E **53**, 157 (1996).

[11] D. Bohm, Phys. Rev. **85**, 166 (1952).

[12] D. Bohm and D. Pines, Phys. Rev. **92**, 609 (1953).

[13] D. Bohm and D. Pines, in *Plasma Physics*, Ed. J. E. Drummond (McGraw-Hill, New York, 1961) Chap. 2, pp. 35–87.

[14] D. Pines, J. Nucl. Energy: Part C: Plasma Phys. **2**, 5 (1961).

[15] E. W. Brown, B. K. Clark, J. L. DuBois, and D. M. Ceperley, Phys. Rev. Lett. **110**, 146405 (2013).

[16] T. G. White, S. Richardson, B. J. B. Crowley, L. K. Pattison, J. W. O. Harris, and G. Gregori, Phys. Rev. Lett. **111**, 175002(2013).

[17] V. Filinov, M. Bonitz, A. Filinov, V. Golubnychiy, Lect. Notes Phys. **739** 41 (2007); arXiv:cond-mat/0611560 [cond-mat.str-el]

[18] Y. L. Klimontovich and V. P. Silin, Doklady Akad. Nauk SSSR **82**, 361 (1952); *ibid.* J. Exp. Teor. Fiz. **23** 151 (1952).

[19] G. Manfredi, Fields Inst. Commun. **46**, 263–287 (2005).

[20] N. Crouseilles, P. A. Hervieux, and G. Manfredi, Phys. Rev. B **78**, 155412 (2008).

[21] P. K. Shukla and B. Eliasson, Rev. Mod. Phys. **83**, 885 (2011).

[22] P. K. Shukla and B. Eliasson, Phys. Usp. **51**, 53 (2010).

[23] P. K. Shukla and B. Eliasson, Phys. Rev. Lett. **108**, 165007 (2012); *ibid.* **108**, 219902 (E) (2012); *ibid.* **109**, 019901(E) (2012).

[24] M. Akbari-Moghanjoughi, Phys. Plasmas **22**, 022103 (2015); *ibid.* **22**, 039904 (E) (2015).

[25] M. Bonitz, E. Pehlke, and T. Schoof, Phys. Rev. E **87**, 033105 (2013).

[26] P. K. Shukla, B. Eliasson, and M. Akbari-Moghanjoughi, Phys. Rev. E **87**, 037101 (2013).

[27] M. Bonitz, E. Pehlke, and T. Schoof, Phys. Rev. E **87**, 037102 (2013).

[28] P. K. Shukla,B. Eliasson and M. Akbari-Moghanjoughi, Phys. Scr. **87**, 018202 (2013); doi:10.1088/0031-8949/87/01/018202

[29] M. Bonitz, E. Pehlke, and T. Schoof, Phys. Scr. **88**, 057001 (2013); doi:10.1088/0031-8949/88/05/057001

[30] D. Michta, F. Graziani, and M. Bonitz, Contrib. Plasma Phys. **55**, 437 (2015).

[31] Z. Moldabekov, T. Schoof, P. Ludwig, M. Bonitz and T. Ramazanov, Phys. Plasmas **22**, 102104 (2015).

[32] F. Haas, *Quantum Plasmas: An Hydrodynamic Approach* (Springer, New York, 2011).

[33] F. Haas and S. Mahmood, Phys. Rev. E **92**, 053112 (2015).

[34] D. B. Melrose and A. Mushtaq, Phys. Rev. E **82**, 056402 (2010).

[35] B. Eliasson and P. K. Shukla, Phys. Scr. **78**, 025503 (2008).

[36] B. Eliasson and M. Akbari-Moghanjoughi, *Finite temperature static charge screening in quantum plasmas* (submitted).

[37] A. Juengel, *Transport Equations for Semiconductors*, (Springer, Berlin 2009).

[38] V. Romano, J. Math. Phys. **48**, 123504 (2007).

[39] L. Stanton and M. S. Murillo, Phys. Rev. E **91**, 033104 (2015).

[40] A. Esfandyari-Kalejahi, M. Akbari-Moghanjoughi, and B. Haddadpour-Khiaban, Phys. Plasmas **16**, 102302(2009).

[41] M. Akbari-Moghanjoughi, Phys. Plasmas **17**, 052302 (2010).

[42] A. G. Stewart and E. W. Laing, J. Plasma Phys. **47**, 295 (1992).

[43] B. Van Zeghbroeck, *Principles of Electronic Devices* (2011), Chap. 2.3.7, http://ecee.colorado.edu/~bart/book/contents.htm

[44] G. P. Zank and R. G. Greaves, Phys. Rev. E **51**, 6079 (1995).

[45] Y. Wang and B. Elasson, Phys. Rev. B **89**, 205316 (2014).

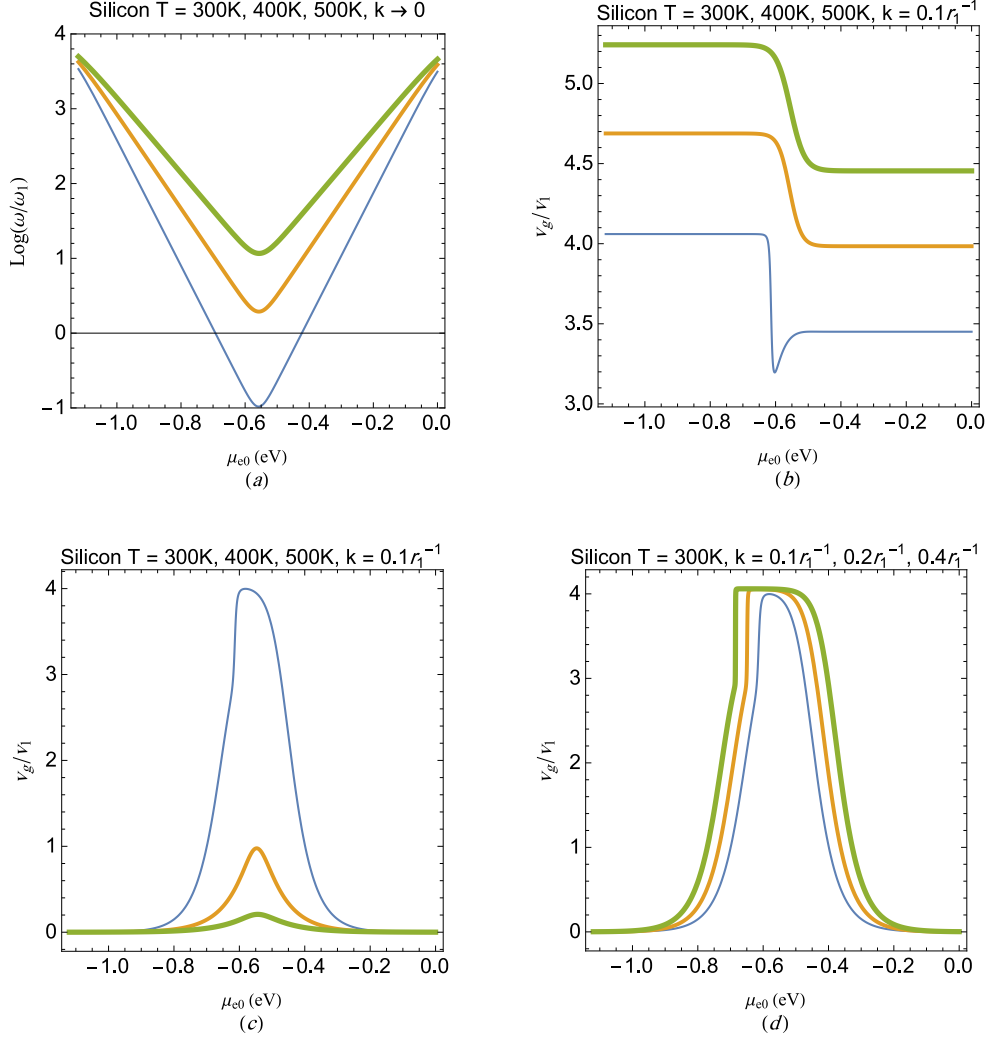[46] S. Ichimaru, H. Iyetomi and S. Tanaka, Phys. Rep. **149**, 91 (1987).

FIG. 4: (a) The long wavelength Langmuir-like branch normalized frequency versus μ_e for different temperatures for a Si sample. (b) The group speed of the acoustic-like branch versus μ_e for different temperatures and $k = 0.1 r_1^{-1}$. (c) The group speed of the Langmuir-like branch versus μ_e for $k = 0.1 r_1^{-1}$ and different values of T. (d) The group speed of Langmuir-like branch versus μ_e for different wavenumbers at $T = 300\,\text{K}$. The subregions $\mu_{e0} < -E_g/2$ and $\mu_{e0} > -E_g/2$ correspond to P- and N-type Si regions, respectively. The normalization factors are $r_1 = 10^{-4}$cm, $\omega_1 = \sqrt{4\pi e^2 n_0/m_0}$ with $n_0 = 10^{12}$cm^{-3} and $v_1 = r_1/\omega_1$. Thicker curves indicate higher values of the temperature listed above each panel.
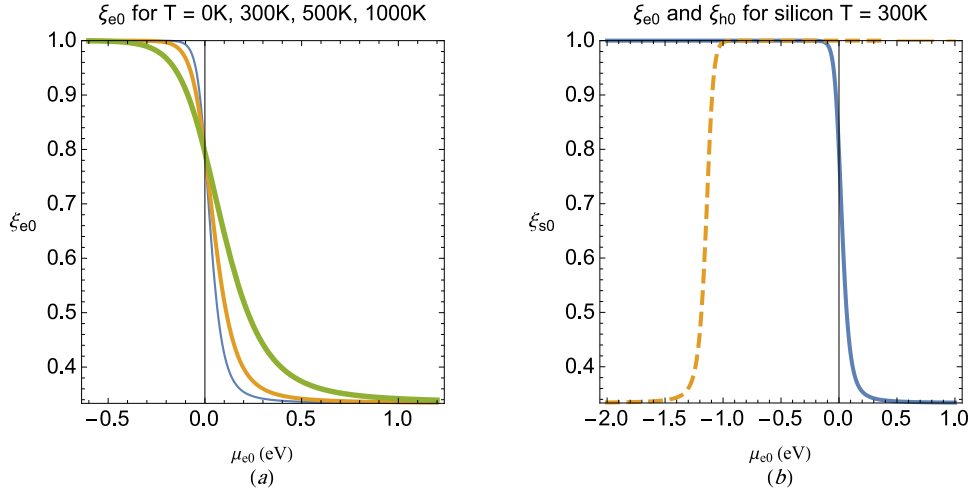
FIG. 5: (a) The low-frequency kinetic correction prefactor ξ_{e0} versus μ_{e0}(eV) for different temperatures. The increase in the thickness of solid profile indicates the increase in the temperature values. The values of $\xi_{e0} = 1$ and $\xi_{e0} = 1/3$ correspond to the classical non-degenerate and fully-degenerate cases, respectively. (b) Comparison between ξ_{e0} (solid) and ξ_{h0} (dashed) at room temperature.
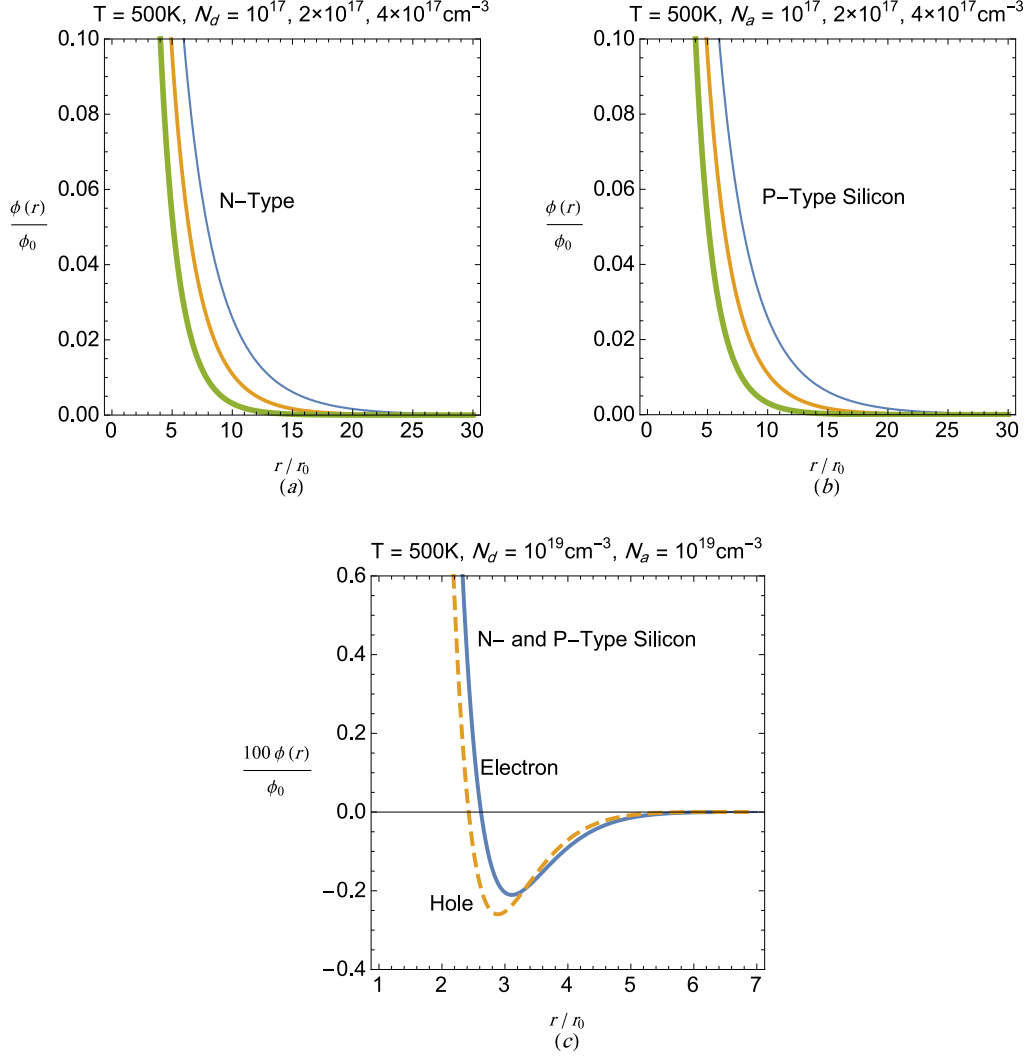
FIG. 6: Profiles of the static charge screening potential by (a) electrons in highly doped N-type Si, (b) holes in highly doped P-type Si. (c) The Shukla-Eliasson-type attractive screening by electrons and holes. The normalization factors used in these plots are $r_0 = 10^{-7}$cm and $\phi_0 = Ze/r_0$. The increase in thickness of curves in panels (a) and (b) indicate the increase in the corresponding doping concentrations above each panel.